Reaction $\bar{p}p \to \bar{p}p\pi^+\pi^-$ Between 1.6 and 2.2 GeV/c*

J. Lys,† J. W. Chapman, and R. Green

The University of Michigan, Ann Arbor, Michigan 48104

and

C. T. Murphy

Carnegie-Mellon University, Pittsburgh, Pennsylvania 15213

(Received 5 July 1972)

The cross section for the reaction $\bar{p}p \to \bar{p}p\pi^+\pi^-$ has been measured at laboratory momenta between 1.62 and 2.20 GeV/c (center-of-mass energy 2294 to 2500 MeV). The cross section rises from 50 ± 16 μb to 975 ± 55 μb in this region, the major rise occurring as the $\bar{\Delta}\Delta$ threshold is crossed around 2465 MeV. The effective mass and angular distributions do not agree well with the one-pion-exchange model of Wolf, which includes off-mass-shell corrections. Various possible causes of the disagreement are discussed.

I. INTRODUCTION

We have studied the reaction

$$\bar{p}p \to \bar{p}p\pi^+\pi^- \tag{1}$$

at six antiproton momenta in the range 1.6 to 2.2 GeV/c in a hydrogen bubble-chamber experiment. The cross section is found to rise from about 50 μb to about 1 mb in this momentum interval. Our effective-mass distributions and production angular distributions suggest that the reaction is dominated by one-pion exchange (OPE). We compare these distributions with the predictions of an OPE model of Wolf.[1] We also compare our results to those of other experimenters at nearby energies.

We also find upper limits to cross sections for those five-body reactions of the type $\bar{p}p \to NN\pi\pi\pi$ that result in four charged particles, i.e.,

$$\bar{p}p \to \bar{p}p\pi^+\pi^-\pi^0, \tag{2}$$

$$\bar{p}p \to \bar{p}n\pi^+\pi^+\pi^-, \tag{3}$$

$$\bar{p}p \to \bar{n}p\pi^+\pi^-\pi^-. \tag{4}$$

II. EXPERIMENT

A. Event Collection

The data come from an exposure of the MURA-Argonne 30-in. hydrogen bubble chamber to an antiproton beam at Argonne National Laboratory. The six antiproton momenta and corresponding center-of-mass energies are listed in Table I. At each incident momentum the momentum spread was 2.4% full width at half maximum (FWHM). Further details about the exposure have already been published.[2]

On approximately one half of the 150 000 pictures, every four-prong interaction was measured. The resulting 50 000 events were processed through the reconstruction and constraint programs TVGP and SQUAW. A total of 442 events fit the four-body hypothesis, reaction (1), with χ^2 probability greater than 10^{-6}. Nearly all fits had four constraints. A bubble-density examination of these events confirmed that all except one were indeed examples of reaction (1).

In addition, another portion of the film was scanned for four-prong events with rules designed to reject many of the multipion annihilations while retaining all nonannihilation events. The incident momentum was sufficiently low that relatively simple scan rules could be applied. For example, at 2.2 GeV/c, at least one of the outgoing protons or antiprotons must have an ionization of greater than 1.6 relative to a minimum-ionizing track and both tracks must lie within 50° of the incident beam direction. This part of the experiment produced 118 new examples of reaction (1) at the two highest momenta. It was verified that these events had the same mass and angular distributions as the first sample. A few rolls processed in both manners were used to determine a scanning efficiency, which was $(92 \pm 3)\%$.

Events at 2.2 GeV/c that did not fit reaction (1) with χ^2 probability greater than 10^{-6}, but whose appropriate missing mass squared was within three standard deviations of zero and had corresponding missing energy between −100 MeV and 100 MeV, were also submitted to the bubble density examination. Nine more examples of reaction (1) were found among these events. These nine events had a definite proton or antiproton track among the outgoing tracks, but were inconsistent with any of reactions (2)–(4). These events were not added to the sample, but cross sections were increased by 4% to correct for the loss.

TABLE I. Numbers of events and cross section for the reaction $\bar{p}p \rightarrow \bar{p}p\pi^{+}\pi^{-}$ as a function of laboratory momentum.

Lab momentum (GeV/c)	1.62	1.76	1.82	1.88	1.94	2.20
Center-of-mass energy (MeV)	2294	2347	2368	2389	2410	2500
From 50 000 4-prong events:						
number of events	10	25	30	61	81	234
cross section (μb)	50± 16	97± 20	125± 23	224± 30	297± 34	937± 65
From scanned sample:						
number of events					20	98
cross section (μb)					241± 60	1080± 116
Weighted-average cross section (μb)					280± 30	975± 55

No measured four-prong events were assigned to reactions (3) or (4). The few events that were kinematically consistent with one of these two reactions were clearly ruled out by the bubble density examination. All those events that fitted reaction (2) and were consistent with the predicted bubble densities (19 events with $\chi^{2} < 6.6$ for the one-constraint fit) also fitted reaction (1), and always the missing mass squared had a large error and was closer to zero than to the square of the π^{0} mass. Hence no events were assigned to reaction (2).
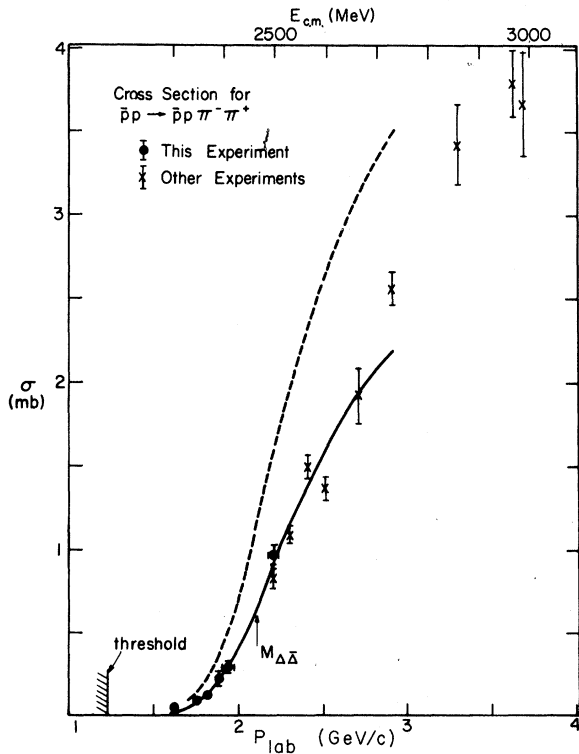
B. Cross Sections

For events arising from the 50 000-event four-prong sample, the ratio of the number of events of reaction (1) to all well-measured four-prong events was multiplied by the independently determined[2] total four-prong cross section to get the cross section at each incident momentum. The numbers of events and the resulting cross sections for reaction (1) are given in Table I. The 4% correction for events with high χ^{2} mentioned in the previous section has been made. The cross-section errors were dominated by the statistical error in the number of events, although the 2% error re-
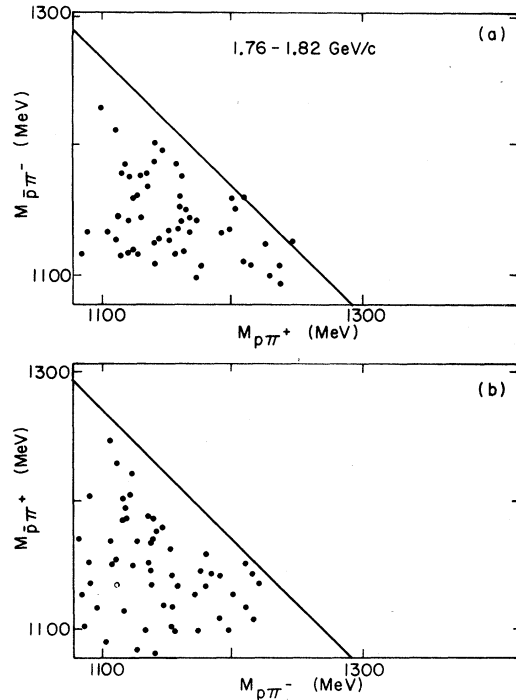

FIG. 1. Cross sections for the reaction $\bar{p}p \rightarrow \bar{p}p\pi^{+}\pi^{-}$, from this experiment and others. The solid curve is the prediction of the one-pion-exchange model described in the text with $R = 2.1$ GeV^{-1}; the dashed curve used $R = 1.76$ GeV^{-1}.

FIG. 2. Scatter plots of (a) $M_{\bar{p}\pi^{-}}$ vs $M_{p\pi^{+}}$ and (b) $M_{\bar{p}\pi^{+}}$ vs $M_{p\pi^{-}}$ for the data at 1.76 and 1.82 GeV/c. The diagonal line is the kinematic limit at 1.82 GeV/c. 55 events.

sulting from the 4% correction factor and the 2.7% errors in the four-prong cross sections have been taken into account.

At 1.94 and 2.20 GeV/c, the cross sections were independently determined from the scanned part of the film, with rolls common with the 50 000 four-prong sample excluded. In this case the cross section was calculated from the number of events, the potential track length (corrected for attenuation in the chamber), and the hydrogen density of $0.062 + 0.002$ g/cm^3. The results were in good agreement with the cross sections from the 50 000 four-prong events. The final line of Table I shows the weighted average cross sections at 1.94 and 2.20 GeV/c.

The cross sections for reaction (1) from this experiment and from other experiments[3-9] are shown in Fig. 1. Measurements have also been made at 5.7,[10,11] 7.0,[12] and 12 GeV/c.[13] The threshold for the reaction occurs at 1.22 GeV/c. The cross section rises rapidly between about 2 and 3.5 GeV/c and then falls off slowly. At

12 GeV/c the cross section is 2.35 ± 0.25 mb. The steep rise occurs at too high a momentum to be responsible for any of the millibarn bumps seen in the antiproton total cross sections around 1.8 GeV/c.[14] The curve on Fig. 1 is the prediction of the OPE model of Wolf discussed in a later section, with the R parameters fixed at values that give reasonable agreement with the cross section at about 2.4 GeV/c.

The absence of any examples of reactions (2)-(4) gives cross-section upper limits for each of these reactions of 4 μb at 2.2 GeV/c, where 4 μb corresponds to one event. Small but nonzero cross sections have been reported for reactions (2)-(4) at 2.4 GeV/c (Ref. 5) and 2.5 GeV/c (Ref. 6) of
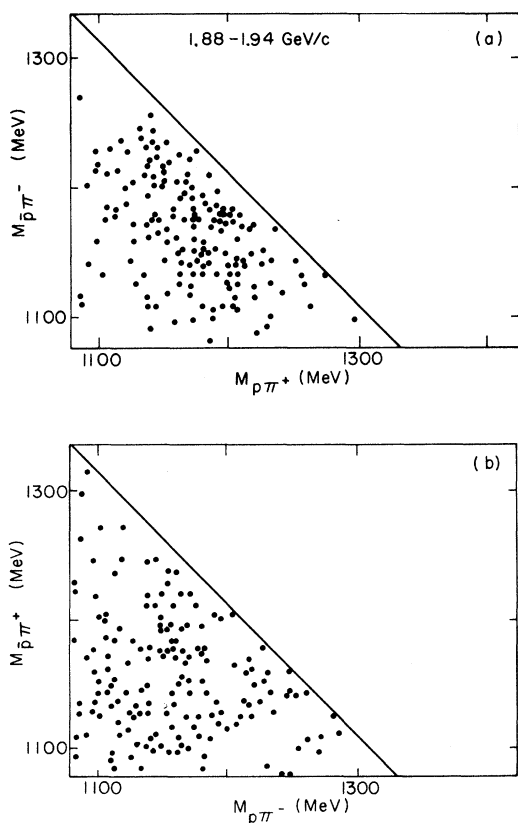

FIG. 3. Scatter plots of the same two-body masses as in Fig. 2 for the data at 1.88 and 1.94 GeV/c. The diagonal line is the kinematic limit at 1.94 GeV/c. 162 events.
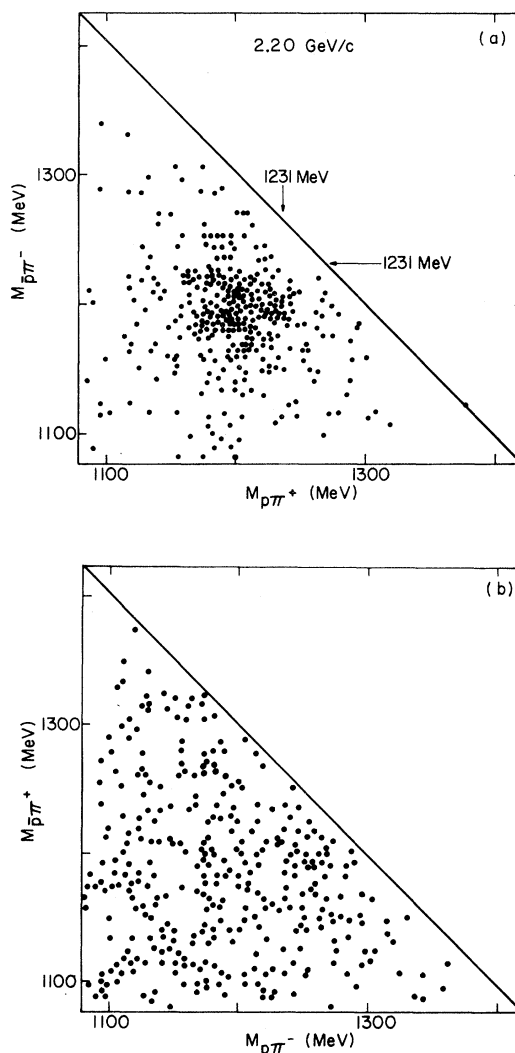

FIG. 4. Scatter plots of the same two-body masses as in Fig. 2 for the data at 2.20 GeV/c. 332 events.
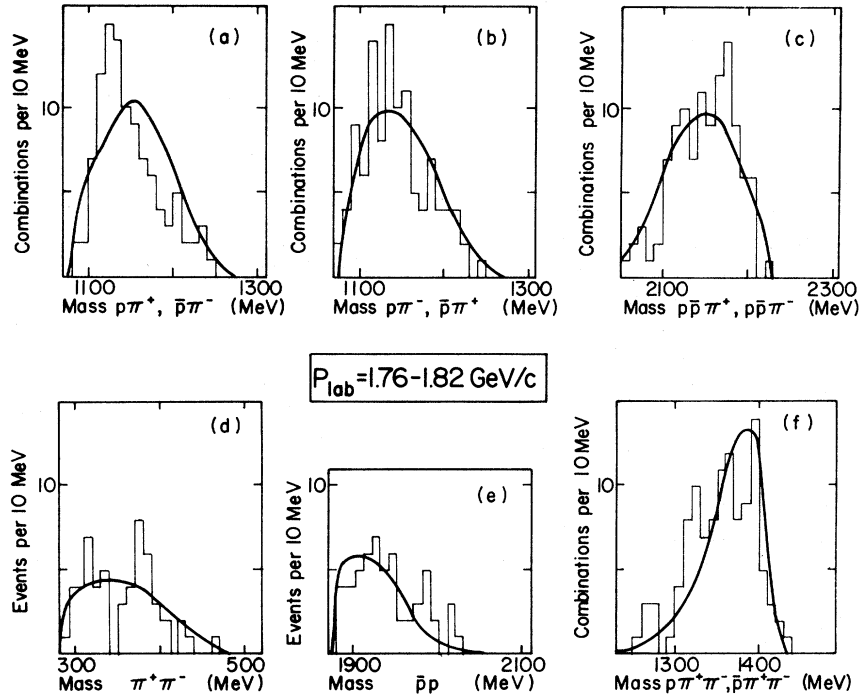
FIG. 5. Mass spectra for the data at 1.76 and 1.82 GeV/c. The curves are the predictions of the one-pion-exchange model (OPE) described in the text. 55 events. Four of the six histograms have two combinations plotted per event.
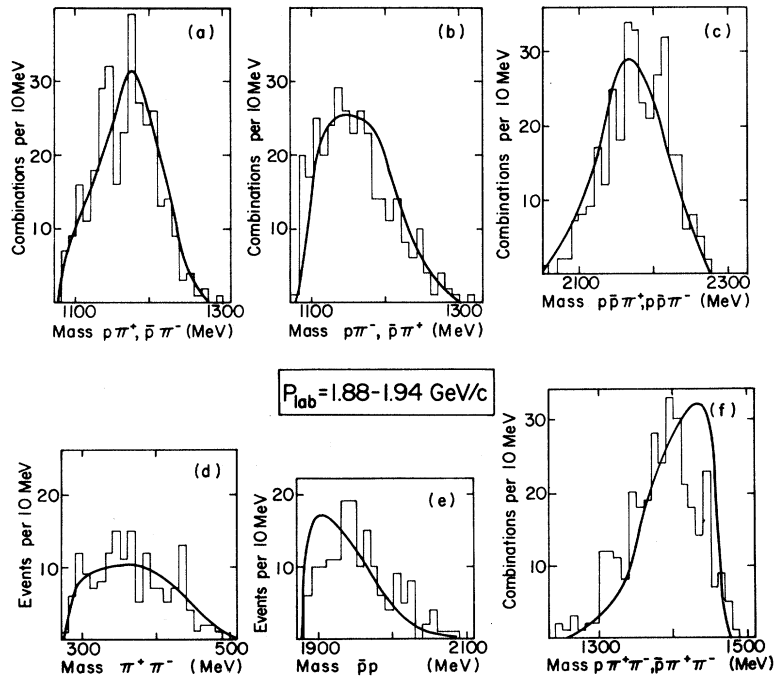

FIG. 6. Mass spectra for the data at 1.88 and 1.94 GeV/c. The curves are the predictions of the OPE model described in the text. 162 events.

around 10 μb. The threshold for these reactions is at 1.63 GeV/c.

C. Experimental Distributions

Figures 2–4 show two-body effective-mass scatter plots of (a) π^+p versus $\pi^-\bar{p}$ and (b) $\pi^+\bar{p}$ versus π^-p for the events at various momenta. In Fig. 4 (2.2 GeV/c) there is a clear difference between the two plots. The concentration of points in Fig. 4(a) with both doubly charged masses near 1200 MeV suggests that the reaction is dominated by $\bar{\Delta}\Delta$ production, as expected from simple OPE models and as seen at higher momenta. At 1.76–1.82 GeV/c (Fig. 2) and 1.88–1.94 GeV/c (Fig. 3), the difference between the two plots is much less noticeable.

Two- and three-body effective-mass plots are shown in Figs. 5, 6, and 7 for the events at 1.76 and 1.82 GeV/c, 1.88 and 1.94 GeV/c, and 2.20 GeV/c, respectively. The solid curves in Figs. 5–9 are predictions of the OPE model of Wolf, normalized to the data, while the dashed curves in Fig. 7 are a variation of the model described later. Distributions in t and $\cos\theta^*$ are shown in Fig. 8 for the same sets of incident momenta, where t is the squared four-momentum transfer from the $\bar{p}$ to the $\bar{p}\pi^-$ system, and $\cos\theta^*$ is the center-of-mass production angle of the $\bar{p}\pi^-$ system with respect to the incident $\bar{p}$.

In Fig. 9 decay angles of the $\bar{p}\pi^-$ and $p\pi^+$ systems in the Jackson frame are shown. The axes are defined in the $\bar{p}\pi^-$ (or $p\pi^+$) rest frame with the incident $\bar{p}$ (or p) along the z axis and the production normal along the y axis, and (θ, ϕ) is the direction of the outgoing $\bar{p}$ (or p). The ϕ distribution at 1.76–1.94 GeV/c (not shown) is similar to that at 2.2 GeV/c shown in Fig. 9(d). The forward-backward asymmetry $(F-B)/(F+B)$ in the $\cos\theta$ distributions and the left-right asymmetry $(L-R)/(L+R)$ in the ϕ distributions are shown in Table II. Here left is defined as $0°<\phi<90°$ and $270°<\phi<360°$, i.e., with the $\bar{p}$ (or p) in the positive x direction. The left-right asymmetry is consistent with zero, while the forward-backward asymmetry is 3 standard deviations from zero, being 0.13 ± 0.04 for the whole data sample. This asymmetry would be zero for a pure spin-$\frac{3}{2}$ decay and suggests a small interference with some other state.

D. Density-Matrix Elements

Despite this nonzero asymmetry, the decay matrix elements were determined for an assumed spin-$\frac{3}{2}$ decay. The decay distribution was written as[15]

$$W(\theta, \phi) = C\{(\tfrac{1}{2} - \rho_{11})\sin^2\theta + \rho_{11}(\tfrac{1}{3} + \cos^2\theta)$$
$$- (2/\sqrt{3})\,\mathrm{Re}\rho_{3,-1}\sin^2\theta\cos2\phi$$
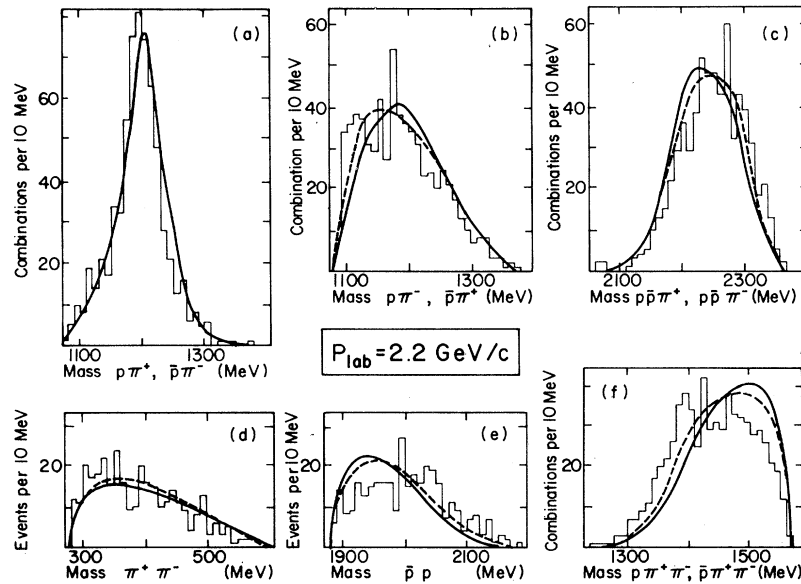$$- (2/\sqrt{3})\,\mathrm{Re}\rho_{3,1}\sin2\theta\cos\phi\} , \qquad (5)$$

FIG. 7. Mass spectra for the data at 2.20 GeV/c. The solid curves are the predictions of the unmodified OPE model described in the text; the dashed curves are an *ad hoc* modification of the same model designed to bring about agreement with the data of Fig. 9(c).
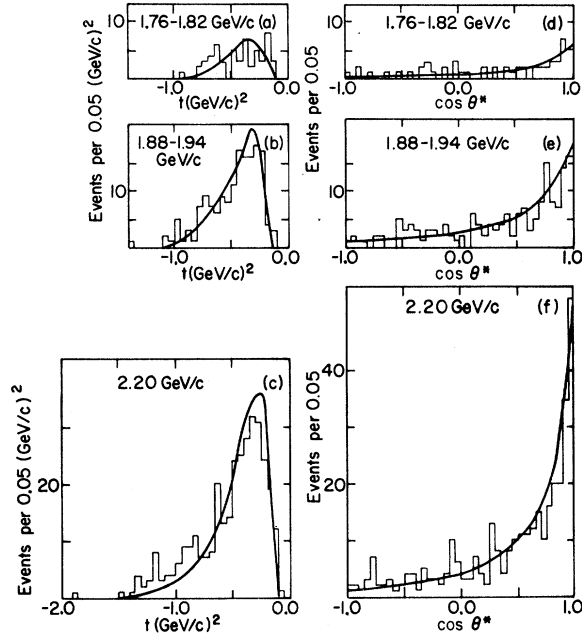
FIG. 8. Production angular distributions ($\cos\theta^*$) and t distributions at various momenta. The angle θ^* is the angle between the incident $\bar{p}$ and the outgoing $\bar{p}\pi^-$ system in the reaction center of mass. The invariant t is the four-momentum transfer from the incident $\bar{p}$ to the outgoing $\bar{p}\pi^-$ system. The curves are the predictions of the OPE model.
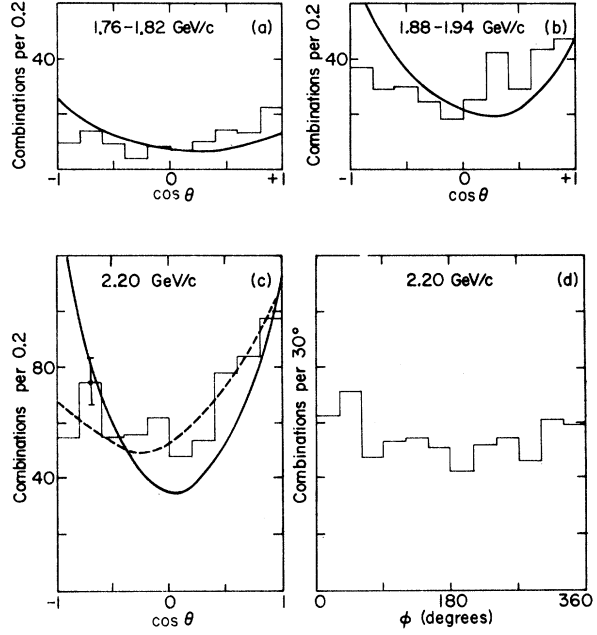

FIG. 9. (a)–(c): Jackson-angle (θ) distributions for various momenta. The angle θ is the angle between the incident and outgoing $\bar{p}$ in the $\bar{p}\pi^-$ rest system, or the same angle in the charge-conjugate system. The solid curves are the prediction of the OPE model. The dashed curve in (c) is the result of the best fit to the $\cos\theta$ distribution at 2.20 GeV/c with mass-dependent shape parameters (see text). (d) Treiman-Yang angle distribution at 2.20 GeV/c. For definition of ϕ, see text.

where C is a normalization constant. The decay matrix elements were evaluated by the maximum-likelihood method for $\bar{p}\pi^-$ and $p\pi^+$ decays combined. The method of moments yielded nearly identical results. The results are given in Table II. The values of $\mathrm{Re}\rho_{3,1}$ and $\mathrm{Re}\rho_{3,-1}$ show no pattern and

are all within 2 standard deviations of zero. The only joint spin-density matrix element[16] evaluated was $b = \frac{1}{2}(\rho^{33}_- - \rho^{11}_-)$, from the average values of $(1 - 3\cos^2\theta)(1 - 3\cos^2\bar{\theta})$. The quantity $b - a^2$, where $a = \frac{1}{2} - 2\rho_{11}$, was found to be within 2 stan-

TABLE II. Density-matrix elements from this experiment and others. The forward-backward asymmetry is the asymmetry in the Jackson-angle (θ) distribution. The left-right asymmetry is the asymmetry in the Treiman-Yang angle (ϕ) distribution. The quantity $b - a^2$, where $a = \frac{1}{2} - 2\rho_{11}$, $b = \frac{1}{2}(\rho^{33}_- - \rho^{11}_-)$, is a measure of the correlation between scattering angles at the two vertices. The first four lines are results of this experiment.

P (MeV/c)	Reference	ρ_{11}	$\mathrm{Re}\rho_{3,1}$	$\mathrm{Re}\rho_{3,-1}$	Asymmetries Forward-backward	Left-right	$b - a^2$
1.62		0.60± 0.12	0.10± 0.12	0.50± 0.10			−0.73± 0.50
1.76–1.82		0.41± 0.06	0.04± 0.06	−0.06± 0.04	0.20± 0.10	−0.04± 0.10	0.06± 0.22
1.88–1.94		0.36± 0.03	0.04± 0.03	−0.03± 0.03	0.15± 0.06	0.09± 0.06	0.18± 0.12
2.20		0.34± 0.02	−0.04± 0.02	−0.02± 0.02	0.09± 0.04	0.06± 0.04	0.05± 0.08
2.2	3	0.28± 0.04	0.06± 0.04	−0.04± 0.04			0.02± 0.10
2.4	5	0.323± 0.013	−0.033± 0.014	−0.028± 0.014	0.068± 0.023	0.074± 0.023	0.031± 0.046
2.5	6	0.335± 0.015	−0.030± 0.015	−0.020± 0.015	0.07± 0.02	0.12± 0.03	
2.7	5, 7	0.348± 0.015	−0.002± 0.015	−0.038± 0.016	0.032± 0.026	0.069± 0.026	−0.005± 0.051
2.9	5	0.308± 0.013	−0.026± 0.012	−0.026± 0.014	0.055± 0.022	0.027± 0.022	0.073± 0.042
12.0[a]	13	0.315± 0.01	−0.01± 0.01	0.02± 0.01	0.098± 0.041	−0.02± 0.04	0.163± 0.09

[a] $M_{\pi^+ p,\, \pi^- \bar{p}} < 1.4$ GeV.

dard deviations of zero, as expected if there is no vertex-vertex correlation.

At 2.2 GeV/c, the matrix elements were evaluated for three different intervals of t. The element ρ_{11} does tend to decrease with large t, but the decrease is not statistically significant.

III. ONE-PION-EXCHANGE MODEL

A. Description

At higher incident momenta reaction (1) has been compared to various versions of the one-pion-exchange (OPE) model. At 12 GeV/c Borecka et al.[13] found good agreement between their mass and momentum transfer distributions and the OPE model of Wolf[1] (OPEW). This model, which Wolf had found to give good agreement with a number of different reactions over a wide incident momentum range, uses Benecke-Dürr[17] form factors to relate the off-mass-shell πp cross sections to on-mass-

shell cross sections. Below 3-GeV/c incident momentum, comparison of OPE with reaction (1) has led to differing conclusions. Bacon et al.[18] and Bomse et al.,[19] in an experiment in deuterium at 2.8 GeV/c, found that their $p\pi^+\pi^-$ and $\bar{p}\pi^+\pi^-$ mass spectra could not be explained by an OPE calculation, and that the $\bar{\Delta}^{--}\Delta^{++}$ final state accounted for only 72% of the reaction. They suggested that a $N^* \to p\pi^+\pi^-$ (and $\bar{N}^* \to \bar{p}\pi^+\pi^-$) resonant state was present in the data. Kernan et al.[20] found that at 2.7 and 2.9 GeV/c the mass spectra were consistent with an OPE calculation with nearly 100% $\bar{\Delta}^{--}\Delta^{++}$. Mason et al.,[6] at 2.5 GeV/c, found that their data required 57% $\bar{\Delta}^{--}\Delta^{++}$ described by OPE plus 43% proceeding via a $\Delta\pi$ interaction, either a $\Delta\pi$ resonance or an s-wave scattering effect.

We have compared our data with OPEW. Absorption and other final-state interactions were not included. The cross section for the diagram of Fig. 10(a) is written as

$$\frac{d^5\sigma}{dt\,dM_1\,dM_2\,d\cos\theta_1\,d\cos\theta_2} = \frac{1}{4\pi^3 p^{*2} s}\,M_1^2 q_{1f}\,\frac{d\sigma(M_1,\cos\theta_1,t)}{d\cos\theta_1}\,\frac{1}{(\mu^2-t)^2}\,M_2^2 q_{2f}\,\frac{d\sigma(M_2,\cos\theta_2,t)}{d\cos\theta_2}\,. \qquad (6)$$

In Eq. (6), s is the square of the total center-of-mass energy, p^* is the momentum of the incident $\bar{p}$ in the center of mass, t is the square of the four-momentum transfer from the proton to the $p\pi^+$ system, μ is the pion mass, M_1 is the mass of the $p\pi^+$ system in the final state, θ_1 is the scattering angle of the proton in the $p\pi^+$ final-state rest frame, and q_{1f} is the momentum of the exchanged pion in the $p\pi^+$ final-state rest frame. M_2, θ_2, and q_{2f} are analogous quantities for the $\bar{p}\pi^-$ final state. The differential cross sections, $d\sigma(M_1,\cos\theta_1,t)/d\cos\theta_1$ and the analogous expression for M_2 and θ_2, are the off-mass-shell cross sections at each vertex, obtained from the equation

$$q_f\,\frac{d\sigma(M,\cos\theta,t)}{d\cos\theta} = F\,\frac{d\sigma(M,\cos\theta)}{d\cos\theta}\,, \qquad (7)$$

where the form factor F is given by

$$F = q\,\frac{(M+m_p)^2-t}{(M+m_p)^2-\mu^2}\,\frac{U_1(q_f R)}{U_1(qR)}\,. \qquad (8)$$

In Eq. (8), q is the momentum of the π^+ (or π^-) in the $\pi^+ p$ (or $\pi^- \bar{p}$) final-state rest frame, m_p is the proton mass, R is a parameter related to the radius of interaction, and U_1 is the function

$$U_1(x) = \frac{1}{2x^2}\left[\frac{2x^2+1}{4x^2}\,\ln(4x^2+1) - 1\right]\,.$$

The cross section $d\sigma(M,\cos\theta)/d\cos\theta$ is the on-mass-shell $\pi^+ p$ (or $\pi^- \bar{p}$) cross section.

Equation (8) is the correct form-factor expression only for the P_{33} partial wave. However, we use the same form factor for all partial waves included in this analysis (S_{13}, P_{13}, P_{33}) for several reasons. First, the form given by Wolf for the s-wave form factor becomes infinite at threshold.[21] Secondly, in the range of M accessible to our experiment ($M < 1423$ MeV at 2.20 GeV/c), the P_{33} partial wave dominates, so the form of F does not matter very much for lower partial waves. Lastly, the mass distributions are not very sensitive to
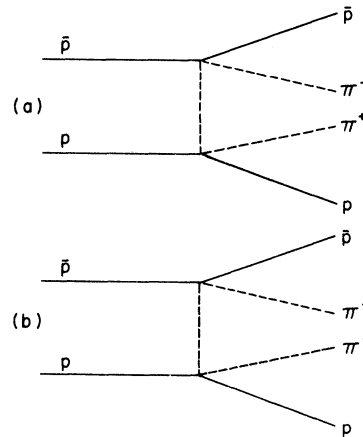

FIG. 10. Feynman diagrams for the two exchange processes included in the OPE model.

the exact form of F, as pointed out by Kernan et al.[20] The function F which we use varies only very slowly with M and t, except when M is very close to threshold. Thus at $M = 1200$ MeV, F is 307 MeV at $t = -0.2$ GeV^2 and 235 MeV at $t = -1.0$ GeV^2.

For the on-mass-shell cross sections in Eq. (7), we use the experimental values as represented by the phase shifts of Roper et al.,[22] except for the P_{33} wave. For the P_{33} wave we use the standard form of the Breit-Wigner curve with $M_\Delta = 1231$ MeV, as suggested by the Particle Data Group.[23]

The cross section for the second OPE diagram, Fig. 10(b), can be written exactly analogously to the first diagram. The two cross sections can then be added incoherently. We have included this second diagram in the total cross section, but it amounts to only 2% of the first diagram (owing to the P_{33} partial-wave dominance) and is neglected in our mass- and t-distribution calculations.

Wolf found 1.76 ± 0.03 GeV^{-1} for the parameter R in fitting $\bar{p}p \rightarrow \bar{\Delta}^{--}\Delta^{++}$ data at 3.6 and 5.7 GeV/c, and the same value gave good absolute agreement at 12 GeV/c. In analyzing the reaction $\pi^+ p \rightarrow \Delta^{++}$, Wolf obtained $R = 2.2$ GeV^{-1}. The value of R affects only the absolute cross sections; the shapes of the mass and t distributions predicted by OPEW are insensitive to small changes in the value of R. In generating mass and t distributions (by Monte Carlo integration) we actually used $R = 2.2$ GeV^{-1} and then normalized the smoothed curves (Figs. 5–9) to the data.

We have compared the predictions of this model with those of Mason et al.[6] at 2.5 GeV/c and those of the Iowa State group[5,7,20] at 2.4, 2.7, and 2.9 GeV/c. While there are large apparent differences between the three models, at these four higher momenta our model yields theoretical mass and t spectra barely distinguishable from those of the other two groups. However, we disagree with the results of the model used by Stringer et al.[24]

B. Comparison of Experiment with OPEW

The solid curve in Fig. 1 is the absolute cross section obtained from Eqs. (6) and (7), with R chosen to be 2.1 GeV^{-1} so as to obtain agreement with experiment near 2.4 GeV/c. The dashed curve corresponds to $R = 1.76$ GeV^{-1}, which Wolf found in analyzing experimental results on the same reaction above 3 GeV/c. If only the P_{33} partial wave is taken into account, the cross section at 2.2 GeV/c is reduced by 13%; at 1.91 GeV/c the cross section is reduced by 21%, and at 1.79 GeV/c by 34%.

The OPEW curve in Fig. 1 shows reasonable agreement with the experimental points below

3 GeV/c. Above 3 GeV/c the calculation requires more than the S and P partial waves which we have used, so the curve has not been extended. However, at 2.9 GeV/c only 6% of the $p\pi^+$ or $\bar{p}\pi^-$ masses are greater than 1400 MeV, so our neglect of higher partial waves should not account for the poor agreement at 2.9 GeV/c. For better agreement at 2.9 GeV/c and at higher momenta, a smaller value of R is required, as expected from Wolf's fits.

We will concentrate our comparison between the experimental distributions and the OPEW calculations on the 2.2-GeV/c data, since at this momentum the number of events is large and there is a reasonable amount of phase space available.

The agreement between the OPEW curves and the data at 2.2 GeV/c (Figs. 7–9) is only fair.

The experimental $p\pi^+$ and $\bar{p}\pi^-$ mass spectrum [Fig. 7(a)] peaks at 1195 MeV, while the OPEW curve peaks at 1210 MeV. Thus the mass shift from the normal 1231-MeV Δ peak, brought about by kinematic factors and the form factors of Eq. (7), is not quite large enough. The excesses of low-mass events in the $p\pi^-$ and $\bar{p}\pi^+$ mass spectrum [Fig. 7(b)] and in the $p\pi^+\pi^-$ and $\bar{p}\pi^+\pi^-$ mass spectrum [Fig. 7(f)] are similar to those seen at 2.5 GeV/c.[6] In addition, the OPEW curves do not fit the $\bar{p}p$ and $\bar{p}p\pi^\pm$ [Fig. 7(c)] spectra very well. The exclusion of S and P_{13} partial waves from the OPEW calculations alter only negligibly the mass-spectra predictions.

At least some of the disagreement between the OPEW and experimental mass spectra may be connected with the experimental, off-mass-shell, $\pi^+ p$ and $\pi^- \bar{p}$ scattering angular distributions [Fig. 9(c)], which disagree violently with the OPE predictions [solid curve, Fig. 9(c)]. At 2.2 GeV/c, OPEW predicts $\rho_{11} = 0.46$ and a forward-backward ratio of -0.07 (averaged over all t), compared to the measured values of 0.34 ± 0.02 and $+0.09 \pm 0.04$, respectively. Comparable disagreement is observed in all other studies of this reaction at any energy.

As an exercise to see whether the disagreements between the OPEW mass distributions and our data are merely a kinematic reflection of the inability of OPEW to fit the decay angular distributions, we have made an ad hoc modification of OPEW by replacing the angular distribution of Eq. (7) with our empirical mass-dependent angular distributions. The mass referred to is the $\pi^+ p$ or $\pi^- \bar{p}$ mass.

The πp scattering angular distributions can be represented by

$$\frac{d\sigma}{d\Omega} = \frac{\sigma}{4\pi} \sum_L \frac{A_L}{A_0} P_L(\cos\theta), \qquad (9)$$

where $P_L(\cos\theta)$ are the conventional Legendre

TABLE III. Shape parameters $(A_1/A_0, A_2/A_0)$ for four intervals in the mass (M) of the $\bar{p}\pi^-$ or $p\pi^+$ system determined from data at $P_{lab} = 2.2$ GeV/c and $P_{lab} = 1.88$–1.94 GeV/c. The first column shows the predictions of the OPEW model at 2.2 GeV/c for all t, where t is the momentum transfer squared from the incident $\bar{p}$ to the outgoing $\bar{p}\pi^-$ system.

t range	P_{lab}	2.2 GeV/c OPEW all t	2.2 GeV/c Experiment all t	2.2 GeV/c Experiment $t>-0.5$	1.88, 1.94 GeV/c Experiment all t	1.88, 1.94 GeV/c Experiment $t>-0.5$
$M < 1150$ MeV	A_1/A_0	-1.02	0.23 ± 0.18	0.40 ± 0.23	0.38 ± 0.17	0.81 ± 0.19
	A_2/A_0	0.66	0.09 ± 0.23	0.29 ± 0.29	0.47 ± 0.21	0.37 ± 0.27
$1150 < M < 1200$ MeV	A_1/A_0	-0.38	0.07 ± 0.11	0.32 ± 0.14	-0.07 ± 0.17	0.18 ± 0.21
	A_2/A_0	0.76	0.20 ± 0.13	0.21 ± 0.16	0.43 ± 0.21	0.44 ± 0.26
$1200 < M < 1250$ MeV	A_1/A_0	0.16	0.34 ± 0.12	0.56 ± 0.16	0.32 ± 0.23	0.40 ± 0.30
	A_2/A_0	0.85	0.57 ± 0.15	0.63 ± 0.21	0.35 ± 0.30	0.63 ± 0.39
$M > 1250$ MeV	A_1/A_0	0.52	0.81 ± 0.22	1.26 ± 0.33	$\cdots$	$\cdots$
	A_2/A_0	1.19	0.32 ± 0.30	1.32 ± 0.42	$\cdots$	$\cdots$

polynomials. The shape parameters A_L/A_0 were evaluated by averaging $P_L(\cos\theta)$ over the experimental distribution:

$$\frac{A_L}{A_0} = (2L+1)\langle P_L(\cos\theta)\rangle .$$

We have evaluated and tabulated these shape parameters up to $L = 2$ for four $\pi^+ p$ and $\pi^-\bar{p}$ intervals, as shown in Table III. For $L = 3$, the shape parameters were consistent with zero. Also given in Table III are the shape parameters predicted by OPEW, which are actually on-mass-shell $\pi^+ p$ scattering shape parameters appropriately averaged over each mass bin. There is a clear disagreement between the experimental values and the values predicted by OPEW.

This same disagreement at low πp masses has been found in other channels where OPE may be dominant, viz., $pp \to p\pi^+ p\pi^-$ at 6.6 GeV/c (Ref. 25) (with $\cos\theta > 0.965$) and $K^+ p \to p\pi^+\pi^- K^+$ at 7.1 GeV/c (Ref. 26) (with $t > -0.5$ GeV^2), as well as in $\bar{p}p \to \bar{p}p\pi^+\pi^-$ around 3.5 GeV/c.[8] Our experimental shape parameters are in at least qualitative agreement with these other experiments, with A_1/A_0 near zero below 1200 MeV and then increasing with mass, and A_2/A_0 positive but smaller than on-mass-shell values.

Quantitatively, our values for A_L/A_0 are in reasonable agreement with those of Colton et al.[25] when we restrict ourselves to low momentum transfer ($t > -0.5$ GeV^2), as did Colton et al. The agreement is much poorer when we impose no cut on t, which suggests a t dependence of the shape parameters.

These shape parameters were folded into OPEW by retaining the mass dependence of the on-shell scattering cross sections, $d\sigma(M, \cos\theta)/d\cos\theta$, but suppressing any angular dependence. The resulting isotropic distribution was then multiplied by the Legendre polynomial sum of Eq. (9). The coef-

ficients A_L/A_0 were represented by linearly increasing functions of M consistent with the results of Table III for all t. The resulting mass and angular distributions are shown as dashed curves in Figs. 7 and 9(c). This ad hoc modification improves the agreement with the experimental data, especially in the $p\pi^-$, $\bar{p}\pi^+$ and $p\pi^+\pi^-$, $\bar{p}\pi^+\pi^-$ distributions [Figs. 7(b) and 7(f)], but only slightly.

That there is any improvement at all is at first thought surprising, since both Kernan et al.[20] and Ferbel et al.[27] found that simpler ad hoc modifications in the angular distribution slightly worsened agreement. Their modification was to change the angular distribution of the πp scattering cross section from $1 + 3\cos^2\theta$ to isotropic. The improved agreement in our experiment results largely from the asymmetry in the $\cos\theta$ distribution, or from the coefficient A_1/A_0, which is always greater than zero. Thus there is an excess of backward π^+ particles from Δ decays which form an excess of low-mass $\bar{\Delta}\pi^+$ events.

It has been noted above that the shape parameters seem to be t-dependent. As a further exercise, one could attempt to improve agreement between theory and experiment by using t-dependent shape parameters. However, we cannot pursue this point further with our limited data. Actually, introduction of t-dependent shape parameters would be the last step we could take in trying to retain the simple OPE picture of Fig. 10 for this reaction. This is so because the $\bar{p}p\pi^+\pi^-$ final state is described by seven variables, our particular choice being t, M_1, M_2, θ_1, θ_2, ϕ_1, and ϕ_2. Our OPE model requires no ϕ_1 or ϕ_2 dependence and requires $d\sigma/d\cos\theta_1$ to be a function only of t, θ_1, and M_1. Continued disagreement with the mass distributions would imply vertex-vertex correlations or some ϕ dependence. In an experiment with larger statistics, one could look directly for any vertex-vertex correlations or ϕ dependence.

C. Possible Causes of the Disagreements

It is seen above that there is disagreement between most experimental mass and angle distributions and the OPEW predictions. We have examined the possibility that the disagreement can be attributed to a difference between off-shell and on-shell πp scattering angular distributions. Such a difference is apparently seen in other reactions. It is not necessarily unexpected, especially at low πp masses, because[25] for fixed πp mass and scattering angle the value of the four-momentum transfer (t_a) from incident to outgoing proton is fixed for on-shell scattering but is a function of t for off-shell scattering. The difference between the on-shell value of t_a and the off-shell values becomes larger at smaller masses.

Other possible causes of the disagreements exist. These include the neglect of absorption, of final-state interactions, of the contribution from the OPE diagram with both final-state pions at one vertex, and of Reggeization.

A special subclass of the neglected OPE diagram, in which a $\Delta\pi$ resonance of mass 1400 MeV is produced at one vertex, is a possibility which has been strongly favored by one group.[18,19] Alternatively, a $\Delta\pi$ final-state interaction described by a scattering length has been considered by Mason et al.[6] It might appear that our spectrum of $p\pi^+\pi^-$ and $\bar{p}\pi^+\pi^-$ masses [Fig. 7(f)] is evidence against a $\Delta\pi$ resonance of mass 1400 MeV, since most of the excess above the OPE curve lies below 1400 MeV. Such is not the case, however, for if one renormalizes the OPEW curve [solid curve, Fig. 7(f)] to the combinations with mass greater than 1480 MeV, the excess is centered at 1390 MeV and constitutes 33% of the data. [At 1.88–1.94 GeV/c, Fig. 6(f), a similar procedure leads to a 40% excess centered at 1370 MeV.]

These fractions are very similar to the fraction (43%) which Mason et al.[6] find they must attribute to $N^*(1400)$ production or $\Delta\pi\bar{p}$ production with $\Delta\pi$ scattering in the final state, having chosen particular models to describe each effect.

A Reggeized OPE model has been compared with experimental data[13] at 12 GeV/c. The agreement was found to be poorer than for the OPEW model.

D. Comparison with Other Experiments

A number of properties of our data are very similar to those found in other experiments on reaction (1) at higher incident momenta. In Table II we give values for the $\Delta(\bar{\Delta})$ decay matrix elements, the forward-backward asymmetry in the $\pi^+ p$ and $\pi^- \bar{p}$ scattering angle, the left-right asymmetry in the Treiman-Yang angle ϕ, and the cor-

relation $b - a^2$, where $b = \frac{1}{2}(\rho_-^{33} - \rho_-^{11})$ and $a = \frac{1}{2} - 2\rho_{11}$. The values at 12 GeV/$c$ came from events with $\pi^+ p$ and $\pi^- \bar{p}$ masses both less than 1400 MeV.

The values of ρ_{11} and the forward-backward asymmetry appear to be remarkably constant. An additional value of ρ_{11} is available, viz., 0.34 ± 0.01 at 5.7 GeV/c for $\pi^+ p$ and $\pi^- \bar{p}$ masses both in the range 1150–1350 MeV. Since ρ_{11} and the forward-backward asymmetry are respectively directly related to the shape parameters A_2/A_0 and A_1/A_0, the mass-averaged shape parameters cannot vary appreciably with incident momentum, although the distribution of masses over which the averaging is done will vary a little with incident momentum. The OPEW model above, with S and P waves (and on-shell shape parameters), predicts a forward-backward asymmetry varying from -0.08 at 2.2 GeV/c to 0.08 at 2.9 GeV/c.

OPE models without absorption predict zero for $\text{Re}\rho_{3,1}$ and $\text{Re}\rho_{3,-1}$. The values in Table II are never more than $2\frac{1}{2}$ standard deviations from zero; however, the values of both are predominantly negative. The left-right asymmetry, which OPE models predict to be zero, is consistently positive below 3 GeV/c.

The quantity $b - a^2$ in Table II is a measure of the correlation between the scattering angles of the two vertices, and is zero for no correlation. Again, while no measurement gives $b - a^2$ more than 2 standard deviations from zero, it is persistently positive.

The various experiments differ only in that the discrepancies between the various mass spectra and OPE (Fig. 7) become progressively worse as the incident momentum becomes lower. For those mass spectra which can be compared from experiments below 3 GeV/c, the discrepancies with OPE are always in the same direction: an excess of low-mass events in the $p\pi^+(\bar{p}\pi^-)$, $p\pi^-(\bar{p}\pi^+)$, $\pi^+\pi^-$, and $p\pi^+\pi^-(\bar{p}\pi^+\pi^-)$ spectra, and an excess of high-mass events in the $p\bar{p}$ and $p\bar{p}\pi^-(p\bar{p}\pi^+)$ spectra.[28] However, at 2.9 GeV/c, none of these discrepancies are statistically significant. Thus OPE fails to fit our data in the same way that if fails to fit data at slightly higher momenta, only more so. This same observation has been made by the Iowa State group[5] in comparing their data at 2.4 and 2.9 GeV/c.

We have not attempted to determine the fraction of our sample which arises from the two-body reaction $\bar{p}p \rightarrow \bar{\Delta}\Delta$, as others have done, since this fraction is quite model-dependent at our energies.

IV. CONCLUSIONS

We have measured the cross section for the reaction $\bar{p}p \rightarrow \bar{p}p\pi^+\pi^-$ at incident $\bar{p}$ momenta in the

range 1.6-2.2 GeV/c. This cross section, whose threshold occurs at 1.22 GeV/c, begins to rise very rapidly around 2 GeV/c. The rapid rise occurs at too high a momentum to account for the bumps observed in the $\bar{p}$ total cross sections.[14] The values of the cross section for this reaction in our momentum range are in quantitative agreement with a one-pion-exchange model if a value for an interaction radius is chosen which is slightly larger than the value required to fit the cross sections for this reaction at higher incident momenta.

The mass and momentum transfer distributions for this reaction at 2.2 GeV/c suggest dominance by one-pion exchange (OPE). We have compared these distributions with the predictions of the OPE model of Wolf,[1] which incorporates Benecke-Dürr form factors for off-mass-shell cross sections. The agreement is only fair. The $\pi^+ p$ and $\pi^- \bar{p}$ scattering angle distributions at the low πp masses accessible in this experiment (mostly less than 1300 MeV) are similar to those observed in other experiments and do not agree with on-mass-shell πp scattering angular distributions. Furthermore, nearly all of the invariant-mass distributions are in disagreement with the above OPE model at 2.2 GeV/c. An *ad hoc* modification of the off-mass-shell πp scattering angular distributions fails to bring the mass distributions into agreement with OPE. The possible causes of the disagreement with OPE are numerous, and include absorption effects, $\Delta\pi$ scattering in the final state, production of $N\pi\pi$ resonances, other neglected final-state interactions, and a t dependence of the off-mass-shell scattering angular distributions. Our data do not rule out the existence of a $\Delta\pi$ resonance at 1400 MeV such as suggested by Bomse *et al.*[19] However, such a resonance has not appeared in subsamples of higher-energy studies of this same reaction selected to contain a single Δ (or Δ^-) and a $\bar{p}\pi^+$ pair (or $p\pi^-$) not in the Δ band.

In comparing our results with those at higher momenta, we find a remarkable constancy in the $\pi^+ p$ and $\pi^- \bar{p}$ scattering-angle distributions, averaged over mass and momentum transfer. The disagreements between our mass spectra and those predicted by OPE are qualitatively the same as those found at 2.4 GeV/c (Ref. 5) and 2.5 GeV/c, (Ref. 6), but are quantitatively larger.

Lastly, we comment that the deviations of our data from OPE may be less surprising than the fact that OPE comes so close to describing the data, at energies which are so little above threshold.

ACKNOWLEDGMENT

*Work supported by the U. S. Atomic Energy Commission.

†Present address: c/o G.P.O., Sydney, Australia.

[1] G. Wolf, Phys. Rev. 182, 1538 (1969).

[2] J. W. Chapman, R. Green, J. Lys, C. T. Murphy, H. M. Ring, and J. C. Vander Velde, Phys. Rev. D 4, 1275 (1971), and references cited therein.

[3] T. A. Stringer, N. Kwak, G. H. Mall, J. E. Manweiler, and R. Stump, Nucl. Phys. B32, 486 (1971) (2.2 GeV/c).

[4] D. S. Rhines, thesis, Argonne National Laboratory Report No. ANL/HEP 7146, 1971 (unpublished) (2.3 GeV/c).

[5] R. A. Jespersen, W. J. Kernan, and R. A. Leacock, Phys. Rev. D 1, 2483 (1970) (2.4, 2.9 GeV/c).

[6] P. Mason, H. Muirhead, A. Poppleton, K. Whiteley, R. Rigopoulos, P. Tsilimigras, and A. Vayaki-Serafimidou, Nucl. Phys. B30, 617 (1971) (2.5 GeV/c).

[7] H. B. Crawley, R. A. Leacock, and W. J. Kernan, Phys. Rev. 154, 1264 (1967) (2.7 GeV/c).

[8] T. Ferbel, A. Firestone, J. Sandweiss, H. D. Taft, M. Gailloud, T. W. Morris, W. J. Willis, A. H. Bachman, P. Baumel, and R. M. Lea, Phys. Rev. 138, B1528 (1965) (3.28, 3.66 GeV/c).

[9] H. C. Dehne, E. Lohrmann, E. Raubold, P. Söding, M. W. Teucher, and G. Wolf, Phys. Rev. 136, B843 (1964) (3.6 GeV/c).

[10] V. Alles-Borelli, B. French, Å. Frisk, and L. Michejda, Nuovo Cimento 48A, 360 (1967) (5.7 GeV/c).

[11] K. Böchmann, B. Nellen, E. Paul, I. Borecka, J. Diaz, U. Heeren, U. Liebermeister, E. Lohrmann, E. Raubold, P. Söding, S. Wolff, S. Coletti, J. Kidd, L. Mandelli, V. Pelosi, S. Ratti, and L. Tallone, Phys. Letters 15, 356 (1965) (5.7 GeV/c).

[12] T. Ferbel, A. Firestone, J. Johnson, J. Sandweiss, and H. D. Taft, Nuovo Cimento 38, 19 (1965) (6.94 GeV/c).

[13] I. Borecka, G. Drews, W. Lenkeit, G. Comai, R. Santangelo, L. Bertanza, A. Bigi, R. Casali, P. Lariccia, R. Pazzi, R. Medves, and C. Petri, Nuovo Cimento 5A, 19 (1971) (12 GeV/c).

[14] R. J. Abrams, R. L. Cool, G. Giacomelli, T. F. Kycia, B. A. Leontic, K. K. Li, and D. Michael, Phys. Rev. D 1, 1917 (1970).

[15] K. Gottfried and J. D. Jackson, Nuovo Cimento 34, 735 (1964).

[16] H. Pilkuhn and B. E. Y. Svensson, Nuovo Cimento 38, 518 (1965).

[17] J. Benecke and H. P. Dürr, Nuovo Cimento 56A, 269 (1968).

[18] T. C. Bacon, F. Bomse, T. B. Borak, W. J. Fickinger, E. R. Goza, E. J. Moses, and E. O. Salant, Phys. Rev.

D 2, 463 (1970).

[19]F. Bomse, E. J. Moses, and T. B. Borak, Nuovo Cimento 68A, 383 (1970).

[20]W. J. Kernan, H. B. Crawley, R. A. Jespersen, and R. A. Leacock, Phys. Rev. D 1, 48 (1970).

[21]The OPE vertex form factors used by Colton et al. (Ref. 25) differ slightly from those of Wolf, so that the S-wave form factor of Colton et al. does not become infinite at threshold. Specifically, Eq. (17e) of Ref. 25 has the term $(M + m_b)$ in both numerator and denominator, while Wolf has $(M \pm m_b)$, where the sign depends on the parity of the πN state.

[22]L. Roper, R. M. Wright, and B. T. Feld, Phys. Rev. 138, B190 (1965).

[23]Particle Data Group, Rev. Mod. Phys. 43, S1 (1971). See p. S114.

[24]Our theoretical t spectrum, Fig. 8(c), disagrees enormously with that of Ref. 3, Fig. 6, which is surprising, since they are analyzing the same reaction at the same laboratory momentum using the same model, OPEW with Benecke-Dürr form factors. Our curve 8(c) fits their data quite well, while their own is a poor fit.

[25]E. Colton, P. E. Schlein, E. Gellert, and G. A. Smith, Phys. Rev. D 3, 1063 (1971).

[26]T. G. Trippe, C.-Y. Chien, E. Malamud, J. Mellema, P. E. Schlein, W. E. Slater, D. H. Stork, and H. K. Ticho, Phys. Letters 28B, 203 (1968).

[27]T. Ferbel, R. Holmes, and S. Stone, Phys. Rev. Letters 22, 1141 (1969).

[28]An exception to this observation is the $p\pi^+$ ($\bar{p}\pi^-$) mass spectrum of Ref. 6, which is in perfect agreement with OPE. However, this agreement results from the fact that the mass of the Δ is a fitted variable in their OPE model. Their fitted value of 1220 MeV is considerably lower than the value 1232 MeV (Ref. 23) used by most authors.

Elastic Scattering and Single-Pion Production in K^+p Reactions at 4.27 GeV/c*

A. Seidl†

The Enrico Fermi Institute and the Department of Physics, University of Chicago, Chicago, Illinois 60637

(Received 12 July 1972)

Elastic K^+p scattering at a beam momentum of 4.27 GeV/c is studied and compared with elastic K^-p scattering in order to extract the imaginary part of the non-Pomeranchukon-exchange amplitude. The single-pion-production cross sections are presented as well as production cross sections and resonance parameters for the $\Delta(1236)$, the $K^{*+}(890)$, and the $K^{*+}(1420)$. Production and decay distributions for the $\Delta^{++}(1236)$ and the $K^{*+}(890)$ are presented and compared with the absorptive particle-exchange model and with Regge-pole-exchange models.

I. INTRODUCTION

The study of states of low multiplicity has yielded much information about the strong interactions.

In this paper we report on elastic scattering and single-pion production as observed in a 7.4-events/μb exposure of the MURA-ANL 30-in. liquid hydrogen bubble chamber to a separated beam of 4.27-GeV/c K^+ mesons. The analysis of similar event topologies at comparable beam momenta can be found in Refs. 1 and 2. Further references can be found in several compilations of K^+-induced reactions.[3,4]

A comparison of K^+p and K^-p elastic scattering yields information on the nondiffractive part of the exchange amplitude.

In the one-pion-production reactions there is copious production of known $K\pi$ and $N\pi$ resonant states. A study of the production and decay properties of these resonant states yields information about the production mechanisms.

In Sec. II of this paper we discuss the collection and reduction of the data. Event selection is discussed in Sec. III. In Sec. IV the elastic scattering data are presented and compared to K^-p elastic scattering at nearby momenta.[5] In Sec. V we present cross sections for the reactions

$$K^+p \to K^+p\pi^0,$$
$$K^+p \to K^0p\pi^+,$$
$$K^+p \to K^+n\pi^+$$

as well as the cross sections for the production of quasi-two-body final states. And, in Sec. VI, we present resonance production and decay distributions and discuss production models for the dominant quasi-two-body final states.

II. THE COLLECTION AND REDUCTION OF THE DATA

The data were collected during two separate exposures of the MURA-ANL liquid-hydrogen bubble